

BitFlipScope: Scalable Fault Localization and Recovery for Bit-Flip Corruptions in LLMs

1st Muhammad Zeeshan Karamat
Bradly Dept. of ECE
Virginia Tech
 Blacksburg, Virginia, USA
 mzeeshan@vt.edu

2nd Sadman Saif
Bradly Dept. of ECE
Virginia Tech
 Blacksburg, Virginia, USA
 sadmansaif@vt.edu

3rd Christiana Chamon
Bradly Dept. of ECE
Virginia Tech
 Blacksburg, Virginia, USA
 ccgarcia@vt.edu

Abstract—Large Language Models (LLMs) deployed in practical and safety-critical settings are increasingly susceptible to bit-flip faults caused by hardware degradation, cosmic radiation, or deliberate fault-injection attacks such as Rowhammer. These faults silently corrupt internal parameters and can lead to unpredictable or dangerous model behavior. Localizing these corruptions is essential: without identifying the affected region, it is impossible to diagnose the source of degradation, apply targeted corrective measures, or restore model functionality without resorting to costly fine-tuning or full retraining. This work introduces BitFlipScope, a scalable, software-based framework for identifying fault-affected regions within transformer architectures under two deployment scenarios. When a clean reference model is available, BitFlipScope performs differential analysis of outputs, hidden states, and internal activations for detecting anomalous behavior indicative of corruption to pinpoint or localize faults. When no reference model exists, it uses residual-path perturbation and loss-sensitivity profiling to infer the fault-impacted region directly from the corrupted model. In both settings, the framework not only enables effective fault diagnosis but also supports lightweight performance recovery without fine-tuning, offering a practical path to restoring corrupted models. Together, these capabilities make BitFlipScope an important step toward trustworthy, fault-resilient LLM deployment in hardware-prone and adversarial environments.

Index Terms—Large Language Models (LLMs), Bit-Flip Faults, Fault Localization, Hardware Fault Injection, Rowhammer Attacks, Model Robustness, Transformer Reliability, AI Security, Fault-Tolerant Machine Learning.

I. INTRODUCTION

The impeccable usability and convenience of Large Language Models (LLMs) have facilitated their widespread adoption in various fields, including education, finance, and medicine. Working with billions of parameters, LLM offers natural language processing, targeted output generation, pattern recognition, and desired information extraction [1]. Given our reliance on LLM outputs across various applications, ensuring the accuracy of these outputs is paramount. Erroneous output from the LLMs in critical systems could lead to severe or catastrophic consequences. Misinformation, hallucination, and trustworthiness are common security concerns and vulnerabilities of LLMs. Gradient-based bit-flip attacks, adversarial attacks, prompt injection, hardware-based attacks, etc., can trigger substantial performance degradation in LLMs' output [2].

Among these attack strategies against LLMs, the bit-flip attack is the most subtle yet damaging, as this strategy targets a small number of the most impactful weights and modifies a single bit for each of those selected weights. This silent corruption of weights causes an unprecedented drop in accuracy for the model's output. This focused manipulation of 10-128 weights among billions of weights can cause a loss of accuracy of 73% on the GPT-2 32-bit model [3]. LLMs are vulnerable to this type of attack through hardware induction as well. The MobileNet-2 model's performance can be compromised to 75% accuracy loss through deterministic bitflips of only 2 weights, leveraging the Rowhammer vulnerability [4].

To initiate countermeasures for reinstating the model's performance, debugging or fault recovery, it is essential to pinpoint exactly which weights have been manipulated by the attack. Existing attack or defense methods lack fine-grained localization as they either quantify global performance degradation or rely on exhaustive parameter comparisons, both of which are infeasible for large-scale models. Given that modern LLMs contain billions of parameters distributed across hundreds of layers, scalable fault localization is an unsolved challenge. In this work, we investigate: how can we design an ideal fault localization tool for LLMs that has (1) granularity, pinpointing faults down to the block, layer, weight and bit level; (2) efficiency, minimizing computational overhead compared to brute-force methods; and (3) scalability, operating feasibly on billion-parameter models without retraining or intrusive architectural modification?

To precisely spot the manipulated bits in an efficient manner requires a particular approach, depending on whether a clean model is available. With access to a clean model and the attacked model for differential settings, comparative parametric analysis can be done. From that, the specific attacked layer, block, weights and bits can be deduced. In most real-world deployments, the clean reference model is not accessible, which complicates pinpointing the source of faults. Consequently, it is crucial to devise methods that can localize bit-flip faults using only a single corrupted model, i.e., in a self-referential setting. In other words, it is also essential to develop a self-referential approach that identifies bit-flip faults directly from just the corrupted model.

In this paper, we present **BitFlipScope**, a unified, software-

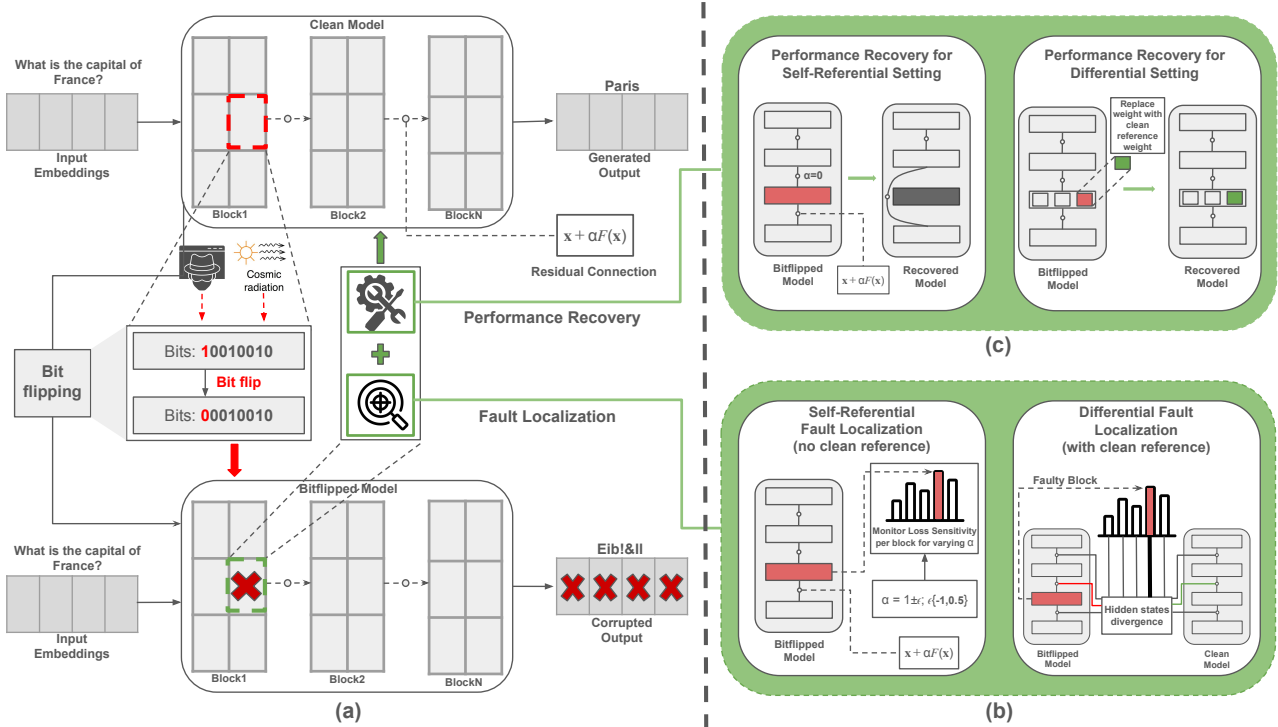


Fig. 1: Overview of the **BitFlipScope** framework for detecting and mitigating bit-flip faults in LLMs. (a) A single bit-flip arising from hardware faults or attack corrupts a transformer block and degrades the model’s output. (b) Fault localization is performed using two approaches: *self-referential* analysis (left), which identifies abnormal loss sensitivity under residual scaling, and *differential* analysis (right), which detects hidden-state divergence using a clean reference model. (c) Once the faulty block is identified, lightweight recovery mechanisms reduce or correct its influence, enabling performance restoration without fine-tuning.

based framework for efficiently localizing and mitigating bit-flip faults in large language models across both differential and self-referential deployment settings. The main contributions of this work are:

- **Dual-setting fault localization:** We propose a unified framework that accurately localizes bit-flip faults both with and without a clean reference model, enabling reliable diagnosis across diverse deployment scenarios.
- **Lightweight performance recovery:** We demonstrate practical, fine-tuning-free mitigation strategies, including targeted parameter restoration in the differential setting and scaling-based attenuation in the self-referential setting.
- **Scalable evaluation:** We validate BitFlipScope across multiple model sizes and corruption sites, showing consistent localization accuracy and substantial performance recovery.

Together, these contributions advance the reliability and security of LLM deployments by enabling practical fault localization and recovery under both constrained and fully informed operating environments.

II. BACKGROUND

This section depicts an overview of different bit-flip attacks against LLMs and neural networks, attack detection and lo-

calization strategies, and performance recovery mechanisms.

A. Bit-flip Attacks

Before discussing about the localization and recovery mechanisms after bit-flip attack, a brief about the attacks highlighted here. Most of the bit-flip attacks are highly focused towards the most vulnerable region of the LLMs using various search strategies to identify parameters whose corruption yields maximal impact. In the case of a hardware-based bit-flip attack against deep neural networks, Progressive Bit Search (PBS) is introduced, where, with gradient search, the most vulnerable bits are ranked in layers and across layers. The corruption of those selected bits is done by leveraging the Row-Hammer vulnerability. With this approach in [5], an accuracy drop from 69.8% to 0.1% was observed after flipping only 13 bits in a ResNet-18 model. In [4], the attack exploits the same vulnerability in DRAM to corrupt quantized DNN model’s weights. Here, a flip-aware bit search algorithm is implemented that not only ranks the most vulnerable bits but also ensures precise bit-flips in the DRAM. 2-24 bit flips would completely compromise the model. This method is implemented on 11 architectures and among those ResNet family showed more resilience as it took more than 20 bit-flips compared to MobileNet-V2, which took only 2 bit-flips for more than 75% accuracy drop. Another approach for physical fault injection

LLWRA [3], showcases a significant accuracy drop in LLMs leveraging row-hammer-based bit-flip attack in Page Frame Number (PFN). The ReBlock algorithm searches for the most impactful block of 128 weights, measuring the gradients. Then that particular block is replaced with another block with minimal bit-flips. This attack manipulated memory addresses with each iteration of block replacement. This achieved an accuracy drop from 78% to less than 5% within 9 iterations on GPT-2 with WikiText dataset.

For the software-based bit-flip approach, in GenBFA [6], the bit-flip attack strategy showcased performance degradation from 67.3% to 0% with 3 bit flips in the LLaMA3-8B-Instruct 8-bit quantized model. They utilized layerwise sensitivity analysis to select the most critical layer, then perturbed weights, dividing them into sets of that particular critical layer to identify the most critical weights in that layer. To minimize the number of bit-flips, again subsets of the selected weights are perturbed to optimize the attack.

Both software and hardware-based attacks demonstrate a significant adverse impact on the model.

B. Localization of the Faults

In all of the attack methods, the most impactful layers, blocks, weights, or bits selection is evident to make the attack efficient and subtle. Localization of the most vulnerable part of the LLM to attack is well-explored which is from an attacker's perspective. In this paper, we examine post-attack fault localization in a deployed LLM model from the perspective of the entity responsible for recovery. In [7], a bit-flip attack detection scheme is demonstrated. In this article, a bit-flip encoding-based detection method is introduced. First, a sensitivity analysis of the quantized neural network's weights determines the most critical ones. These selected weights are encoded with a secret key into a binary detection code. These sensitive weights are monitored by continuously computing the Hamming distance between the current detection code and the securely stored code. Large Hamming distance dictates that there has been an attack.

But this scheme does not pinpoint exact bits or weights that have been manipulated. Whether a model is attacked or not can be detected by analyzing the output of that model. To the best of our knowledge, no prior work provides a practical, scalable tool to localize bit-flip faults in LLMs at block/layer/weight/bit granularity. This paper presents an efficient, fine-grained localization approach that works both with and without access to the fault-free reference model, potentially enabling the development of new recovery strategies for compromised models.

C. Performance Recovery Techniques After Bit-flip Attack

With the goal of introducing a resilient transformer-based model, in [8], a unique architecture is demonstrated called Forget and Rewire. This approach finds out ineffective weight parameters using sensitivity analysis based on the gradients of the weights. After identifying those dead weights, this algorithm forgets them and rewrites those configurations of

inputs with a division factor that dilutes the gradient of a significant weight by half. From the attackers' perspective, the weight rankings change, and the attackers need to flip more bits than before to do the same performance degradation. With this scheme implemented, the model's performance drop no more than 2%. Another approach called NeuroPots [9] introduces a proactive defense mechanism for neural networks. This mechanism adds honey neurons, which are enhanced activation values with an expanding coefficient that puts these neurons up in the weight ranking to attack. These particular neurons will be monitored, and if the attack is detected, then securely stored clean honey weights will be replaced by clean ones. The model's accuracy can be restored to 90% after mitigation. In [10], a fault tolerance technique is showcased for Vision Transformers where, the Least Significant Bit of all parameters are replaced with parity bit and forced to have an even parity. This works as an error detection system when a bit is flipped, then in the parity check, a flag is raised as an attack. The affected parameter is zeroed out. This mechanism can keep ViT's accuracy above 85% with a threshold Bit Error Rate of 2e-5.

These fault detection and recovery techniques are implemented and tested in neural networks or small-scale transformers, whereas large-scale LLMs have billions of parameters, and bit-flip attacks on them exhibit a more subtle yet progressively degrading effect. These still leave a research gap in pinpointing the location of a bit-flip attack and recovery technique using the attacked LLM. Targeting to fill that gap, BitFlipScope introduces recovery mechanisms, both differential and self-referential settings, that complement these architectural defenses by enabling post-attack localization and recovery of bit flips without requiring retraining, auxiliary neurons, or pre-embedded fault-tolerant structures.

III. METHODOLOGY

The overall BitFlipScope workflow is illustrated in Fig. 1. In practice, bit-flip faults may arise under two distinct deployment scenarios: (i) a *differential* setting, where a clean reference model is available, and (ii) a *self-referential* setting, where only the corrupted model can be accessed. These scenarios differ fundamentally in the information available for diagnosis and motivate the two complementary localization paths in our framework.

Accordingly, this section is organized into three parts. We first formalize the two fault-localization settings. We then describe the localization methodology for each case. Finally, we present the lightweight performance recovery mechanisms that use the localized fault information to restore model behavior without fine-tuning.

A. Fault Localization Settings

a) Differential Setting: In some deployments, a clean reference model may be preserved in secure storage, mirrored across nodes, or retrievable from a verified checkpoint. This setting allows behavioral comparison between the corrupted

and clean models. The challenge lies in performing such comparison efficiently, without relying on infeasible parameter-level diffing across billions of weights.

b) Self-Referential Setting: In many realistic scenarios edge deployments, memory-constrained systems, or models updated in-place—only the corrupted model is available. No checkpoints or clean replicas can be accessed, and the system must diagnose faults from the corrupted model alone. This scenario is significantly more challenging, because no ground-truth behavior is available for comparison. Our method addresses this by exploiting structural properties of transformer architectures to infer abnormal computation patterns without any external reference.

B. Self-Referential Fault Localization

Transformer blocks contribute to the forward computation through residual pathways. Assuming the input to the i -th transformer block is \mathbf{h}_i , the block output can be expressed as a composition of its attention and feed-forward components, each equipped with a residual pathway. Following the standard transformer formulation [11], the block computes:

$$\mathbf{h}_{i+1} = \mathbf{h}_i + \underbrace{\text{ATTN}_i(\mathbf{h}_i)}_{\text{self-attention}} + \underbrace{\text{MLP}_i(\mathbf{h}_i + \text{ATTN}_i(\mathbf{h}_i))}_{\text{feed-forward}},$$

where $\text{ATTN}_i(\cdot)$ and $\text{MLP}_i(\cdot)$ denote the attention and feed-forward transformations, respectively. Both submodules contribute additively through residual connections, forming the dominant pathway through which information propagates across the depth of the model.

Because residual connections directly control the influence of each block on subsequent computations, scaling the residual contribution of block i by a factor α_i effectively modulates the distribution of its output:

$$\mathbf{h}_{i+1} = \mathbf{h}_i + \alpha_i F_i(\mathbf{h}_i).$$

where $F_i(\cdot)$ is the block’s transformation (self-attention and MLP components). When $\alpha_i > 1$, the block’s contribution is amplified, increasing the magnitude of its output and correspondingly affecting the input to block $i+1$ during inference. This amplification changes the distribution of the hidden-state vector and effectively strengthens the block’s role in the autoregressive token-generation process. Conversely, when $\alpha_i < 1$, the block’s influence is diminished, reducing its contribution to the model’s forward computation. Applying such scaling across blocks similarly increases or decreases their collective effect on the resulting output distribution. This controllable adjustment of the block’s output distribution forms the foundation of our self-referential localization approach.

a) Residual Perturbation: To identify corrupted blocks, we probe the model’s behavior under controlled deviations of the scaling parameter α_i from its nominal value of 1, following the procedure summarized in Algorithm 1. For each block, we evaluate the model after slightly increasing its residual contribution (*scale-up*: $\alpha_i = 1 + \epsilon$) and slightly decreasing it (*scale-down*: $\alpha_i = 1 - \epsilon$). In a healthy block, such small

Algorithm 1: Self-Referential Fault Localization via Residual Sensitivity

Input: Faulty model M_{faulty} , Input set \mathcal{X} , Scaling set \mathcal{A}
Output: Suspected faulty block B^*
foreach block i in the transformer **do**
 Initialize sensitivity score $S_i \leftarrow 0$;
 foreach $\alpha \in \mathcal{A}$ **do**
 Temporarily set residual scaling of block i to α ;
 Compute loss $\mathcal{L}_{i,\alpha}$ of M_{faulty} on \mathcal{X} ;
 Update sensitivity score: $S_i \leftarrow S_i + |\mathcal{L}_{i,\alpha}|$;
 Reset block i scaling to $\alpha = 1$;
 $B^* \leftarrow \arg \max_i S_i$;
return B^*

adjustments produce only minor and predictable changes in the model’s output distribution. However, when a block’s internal parameters have been corrupted by a bit-flip, these adjustments expose its abnormal influence: increasing α_i strengthens the effect of the corrupted transformation, while decreasing α_i weakens it. This asymmetric behavioral response provides the foundation for detecting the presence of a faulty block.

b) Loss Change Metric: To quantify how each block responds to residual scaling, we measure the change in model loss induced by different values of α_i . For block ℓ , we define the loss change as:

$$\Delta \text{Loss}(\ell, \alpha) = \text{Loss}(\ell, \alpha) - \text{Loss}_{\text{base}},$$

where $\text{Loss}_{\text{base}}$ denotes the loss under the unscaled model ($\alpha = 1$). This quantity captures how strongly the model’s output distribution shifts when the influence of block ℓ is amplified or attenuated. Blocks whose computations are intact yield small and consistent ΔLoss values, whereas corrupted blocks exhibit disproportionately large deviations. This metric provides the quantitative foundation for identifying abnormal block behavior.

c) Selecting Scaling Values via an α -Sweep: Before performing localization, we conduct an α -sweep to determine which scaling values provide the most informative response for detecting faulty blocks. For a representative block, we vary the scaling parameter across a broad range, $\alpha \in [0.2, 1.8]$, and compute the corresponding loss change $\Delta \text{Loss}(\ell, \alpha)$ for each value. As shown in Fig. 2, the loss changes markedly near moderate scaling adjustments but flattens for values outside the approximate interval $[0.6, 1.4]$.

Values below 0.6 excessively suppress the block’s contribution, saturating its effect and yielding negligible diagnostic variation. Likewise, values above 1.4 amplify the block’s output to the point where further increases in α do not produce meaningful changes in loss. Both extremes therefore provide limited sensitivity for distinguishing healthy blocks from corrupted ones. Based on this empirical observation, we restrict our analysis to scaling factors within the interval

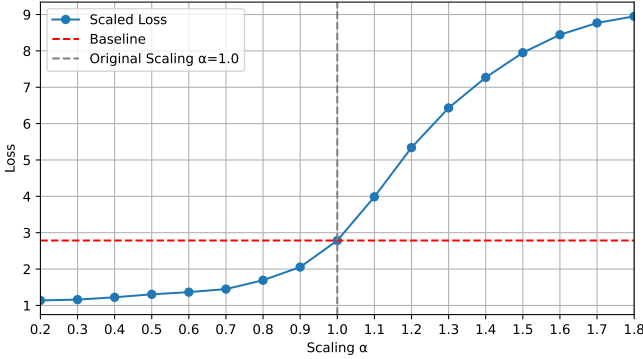


Fig. 2: Loss change ΔLoss across a broad range of scaling values $\alpha \in [0.2, 1.8]$ for a representative block. Diagnostic sensitivity is highest in the interval $[0.6, 1.4]$, which motivates the selection of scaling values used in subsequent experiments.

$[0.6, 1.4]$, where the model exhibits the strongest and most stable response to residual modulation. In practice, we use the discrete set

$$\alpha \in \{0.6, 0.7, 0.8, 0.9, 1.1, 1.2, 1.3, 1.4\},$$

which provides a fine-grained sweep on both sides of the nominal value $\alpha = 1.0$ while avoiding saturated or insensitive regions of the loss curve. These scaling values offer a balanced view of attenuation and amplification, enabling robust detection of anomalous block behavior.

d) Sensitivity Metric: After computing the loss change for each block across the selected scaling values, we aggregate these responses into a single score that reflects how strongly each block reacts to residual modulation. Let \mathcal{A} denote the set of scaling factors chosen from the α -sweep. For block ℓ , we define the Block Sensitivity Score (BSS) as:

$$\text{BSS}(\ell) = \sum_{\alpha \in \mathcal{A}} |\Delta\text{Loss}(\ell, \alpha)|,$$

which can be expanded using the loss-change definition as:

$$\text{BSS}(\ell) = \sum_{\alpha \in \mathcal{A}} |\text{Loss}(\ell, \alpha) - \text{Loss}_{\text{base}}|$$

Blocks whose computations are intact exhibit small and consistent sensitivity scores because their loss remains largely stable across the selected α values. In contrast, a corrupted block yields a distinctly higher score, reflecting the amplified effect of scaling on its abnormal output distribution. We therefore identify the block with the highest BSS as the anomalous and thus likely faulty block. This metric is lightweight, fully gradient-free, and exploits predictable error propagation patterns induced by bit-level corruption.

C. Differential Fault Localization

When a clean reference model is available, fault localization can leverage direct behavioral comparison between the faulty and uncorrupted models. We refer to this setting as *differential fault localization*. The central idea is to treat the clean

Algorithm 2: BitFlipScope: Differential Fault Localization

Input: Clean model M_{clean} , Faulty model M_{faulty} , Input set \mathcal{X}

Output: Faulty block B^* , layer L^* , bit indices β^*

Stage 1: Block Localization
 $B^* \leftarrow \text{LocalizeBlock}(M_{\text{clean}}, M_{\text{faulty}}, \mathcal{X})$

Stage 2: Layer Localization
 $L^* \leftarrow \text{LocalizeLayer}(M_{\text{clean}}, M_{\text{faulty}}, B^*, \mathcal{X})$

Stage 3: Weight and Bit Localization
 $\beta^* \leftarrow \text{LocalizeWeightAndBit}(M_{\text{clean}}, M_{\text{faulty}}, B^*, L^*)$

return (B^*, L^*, β^*)

Function $\text{LocalizeBlock}(M_{\text{clean}}, M_{\text{faulty}}, \mathcal{X})$:
 Compare hidden states of all transformer blocks using cosine similarity or ℓ_2 distance.
return block with maximum deviation.

Function $\text{LocalizeLayer}(M_{\text{clean}}, M_{\text{faulty}}, B^*, \mathcal{X})$:
 Extract activations from attention and MLP layers within B^* .
 Compute similarities to identify layer with lowest agreement.
return suspect layer L^* .

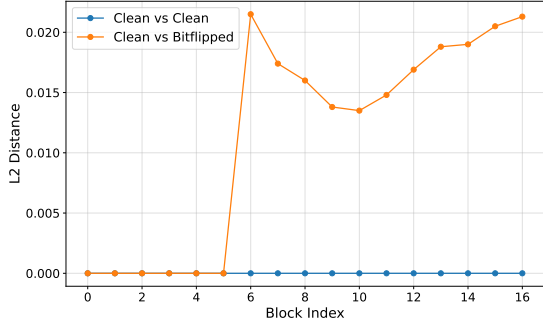
Function $\text{LocalizeWeightAndBit}(M_{\text{clean}}, M_{\text{faulty}}, B^*, L^*)$:
 Compute hash for each parameter tensor in L^* .
 Identify tensors with differing hashes and compare element-wise.
 Locate flipped bits and return indices β^* .

model as an oracle representing correct functionality and to identify divergences in intermediate representations as the bit-flip propagates through the transformer stack. Our approach, summarized in Algorithm 2, performs this diagnosis in three progressively finer stages: block-level localization, layer-level localization, and weight/bit-level localization.

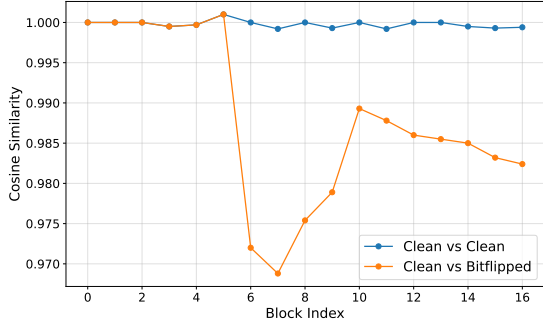
1) Stage 1 - Transformer Block Localization: Each transformer block comprises a self-attention module and a feed-forward MLP module. A bit-flip injected into either component perturbs the block’s output, which in turn propagates through the remaining layers. To identify the affected block, we compare the hidden states produced by the clean and corrupted models at each block boundary. Formally, for an input set \mathcal{X} , we extract the hidden states $\{h_i^{\text{clean}}\}_i$ and $\{h_i^{\text{faulty}}\}_i$ and compute their discrepancy using cosine similarity [12] or ℓ_2 distance [13].

Similarity metrics operate directly on the high-dimensional hidden vectors and are therefore sensitive to localized perturbations, unlike perplexity or entropy, which average over entire sequences. This enables clear detection of abnormal deviations. As illustrated in Fig. 3, the block containing the injected bit-flip exhibits a sharp drop in similarity and a

corresponding spike in distance. The block with the maximum deviation is selected as the candidate faulty block B^* .



(a) Block-wise ℓ_2 distance between clean-clean and clean-faulty pairs, showing a spike at the corrupted block 5.



(b) Block-wise cosine similarity showing a sharp drop at the corrupted block 5.

Fig. 3: Hidden-state comparison between clean and bit-flipped models for block-level localization.

2) *Stage 2 - Layer Localization*: After identifying the faulty block, we isolate the corrupted component by comparing internal activations of its sublayers. Using forward hooks, we extract activations from the self-attention and MLP layers of both models for each input in \mathcal{X} . We compute similarity between corresponding activations; the sublayer exhibiting the lowest similarity is selected as the faulty layer L^* .

This technique, which we refer to as *activation fingerprinting*, provides a fine-grained diagnostic signal. Because all other blocks and layers remain uncorrupted, differences are highly localized and interpretable. Fig. 4 demonstrates that the corrupted layer produces a distinct drop in cosine similarity relative to the clean model.

a) *Efficiency*: Activation fingerprinting is computationally efficient. Instead of scanning millions of weights, it compares a small number of layer-wise activations, avoiding brute-force search while remaining fully non-invasive.

3) *Stage 3 - Weight and Bit Localization*: Once the faulty layer is identified, we locate the corrupted parameter tensor and the specific flipped bit(s). A direct element-wise comparison of parameters is infeasible for large LLMs, so we employ a two-step approach.

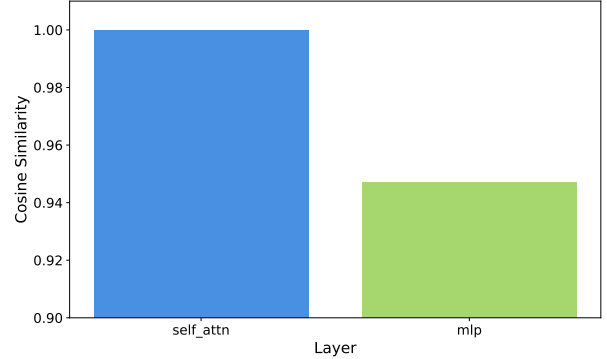


Fig. 4: Cosine similarity of attention vs. MLP layer activations within the faulty block. The corrupted layer mlp in this case exhibits a drop in similarity.

a) *Parameter Hashing*: For each tensor in the suspected layer, we compute a hash value (e.g., SHA-1) for both the clean and corrupted models [14]. Tensors whose hashes match are guaranteed to be identical and can be skipped. Only tensors with differing hashes are examined further, dramatically shrinking the search space.

b) *Bit-Level Comparison*: For tensors with mismatched hashes, we perform an element-wise comparison to identify which parameter value differs between the two models. We then locate the exact bit indices β^* responsible for the mismatch. This yields the final localization result (B^*, L^*, β^*) .

Differential fault localization exploits the clean model as an oracle to progressively narrow the search, from blocks, to layers, to specific parameter tensors, and ultimately to individual bit flips. This multi-resolution analysis provides precise and interpretable localization while avoiding brute-force search over billions of parameters.

D. Performance Recovery

Once the corrupted block has been identified, BitFlipScope applies lightweight performance recovery mechanisms to mitigate the impact of the fault without requiring fine-tuning or retraining. An overview of the recovery stage is shown in Fig. 1(c). The recovery strategy differs slightly depending on whether a clean reference model is available.

a) *Self-Referential Setting*: When no clean reference model exists, we cannot directly restore corrupted parameters. Instead, we employ inference-time adjustment mechanisms that reduce the influence of the faulty block on the model's forward computation. Specifically, we leverage the same residual-scaling mechanism used for localization: by attenuating the corrupted block's residual contribution, the model's predictions can be stabilized and partially corrected. This approach selectively suppresses the block's abnormal computation while leaving the remaining network unchanged, providing a practical and low-cost mitigation method suitable for real-world deployments where reference models or retraining resources may be unavailable.

b) Differential Setting: When a clean model is available, BitFlipScope can undertake more targeted recovery. After the corrupted block and faulty sublayer are identified, the parameters of the clean model serve as a ground-truth reference that allows us to restore the affected tensors directly. This correction is performed at the granularity indicated by the localization stage, replacing only the corrupted parameters while preserving all other weights. This targeted restoration avoids the need for global retraining, restores the model’s functional behavior, and ensures minimal disruption to the remaining computation graph.

IV. EXPERIMENTS

We evaluate BitFlipScope under realistic hardware-fault conditions using a state-of-the-art transformer model subjected to adversarial bit-flip perturbations. Our experiments are designed to assess (1) the accuracy of fault localization under both differential and self-referential settings, and (2) the reliability of the behavioral signals used for diagnosis.

A. Model and Hardware Configuration

All experiments use the **LLaMA 3.2 3B** model in 8-bit quantized form. We select this model because it is fully open-source, supports direct weight inspection for controlled bit-flip injection, and provides a realistic yet computationally manageable LLM scale for repeated fault-injection experiments. Its architecture is also representative of larger transformer models [15], making our findings broadly generalizable.

The 8-bit variant is chosen because quantization amplifies the impact of bit-flip faults: with fewer bits per weight, a single flip induces a larger numerical deviation and more pronounced activation distortion, making it an ideal setting for evaluating localization robustness. All experiments are conducted on an NVIDIA RTX 6000 Ada GPU (48 GB).

B. Dataset and Evaluation Metrics

We use the Massive Multitask Language Understanding (MMLU) benchmark [16] to evaluate the model before and after fault injection. MMLU spans a diverse collection of multiple-choice tasks across 57 subject areas, including mathematics, history, law, computer science, and the natural and social sciences. This diversity is well-suited for our study: bit-flip faults may manifest differently depending on the semantic and reasoning demands of the input, and a broad evaluation ensures that we capture fault effects across heterogeneous cognitive workloads rather than a narrow task domain.

Performance is measured using two metrics:

- **Accuracy**, the fraction of correctly predicted answers across all tasks.
- **Cross-Entropy Loss**, computed as the negative log-likelihood of the correct answer [17].

Together, these metrics provide both coarse (accuracy) and fine-grained (loss) indicators of degradation, enabling precise assessment of the model’s behavioral changes under bit-flip fault injection.

C. Bit-Flip Injection

To introduce controlled and realistic bit-level corruptions, we use the GenBFA methodology [6] solely as a mechanism for selecting which weight bits to flip. GenBFA identifies *critical* parameter locations by analyzing weight magnitude and gradient sensitivity, ensuring that the injected faults meaningfully affect model behavior. This selection criterion is general to any fault-injection framework and does not influence or constrain our localization approach; BitFlipScope operates independently of the specific method used to choose the flipped bits.

In our experiments, fewer than 3% of the candidate weight bits identified by GenBFA are actually flipped, allowing us to inject minimal but high-impact perturbations that closely reflect real-world hardware faults such as radiation-induced single-bit errors or targeted fault-injection attacks. Each experiment flips a bit at one of these critical locations, producing a corrupted model instance for evaluating our localization and recovery techniques.

D. Evaluation Under Two Reference Settings

We evaluate BitFlipScope in both deployment scenarios introduced in Section III. In the *differential setting*, where a clean reference model is available, localization accuracy is measured by comparing the fault identified by BitFlipScope with the ground-truth corrupted block, sublayer, and parameter. In the *self-referential setting*, where only the corrupted model is available, we assess the ability of residual-scaling-based sensitivity analysis to isolate the faulty block without access to clean activations. Both evaluations are performed across multiple model sizes and corruption sites.

E. Experimental Goals

Our experiments aim to answer the following questions:

- **Localization Accuracy:** Can BitFlipScope consistently identify the corrupted block or sublayer following a targeted bit-flip?
- **Signal Quality:** Do hidden-state divergences and residual-scaling sensitivities provide clear and separable diagnostic signatures?
- **Robustness Across Models and Fault Sites:** Are localization signals stable across different model sizes, block depths, and corruption locations?
- **Recovery Readiness:** Does accurate localization enable lightweight, non-finetuned performance recovery in both differential and self-referential settings?

V. RESULTS

We evaluate BitFlipScope under both localization settings described in Section III. Our results examine (i) how reliably the self-referential approach identifies corrupted blocks using loss sensitivity under residual scaling, (ii) how accurately the differential approach localizes faults at the block and sublayer levels, and (iii) how the computational cost compares to brute-force search. We present results for the two settings separately,

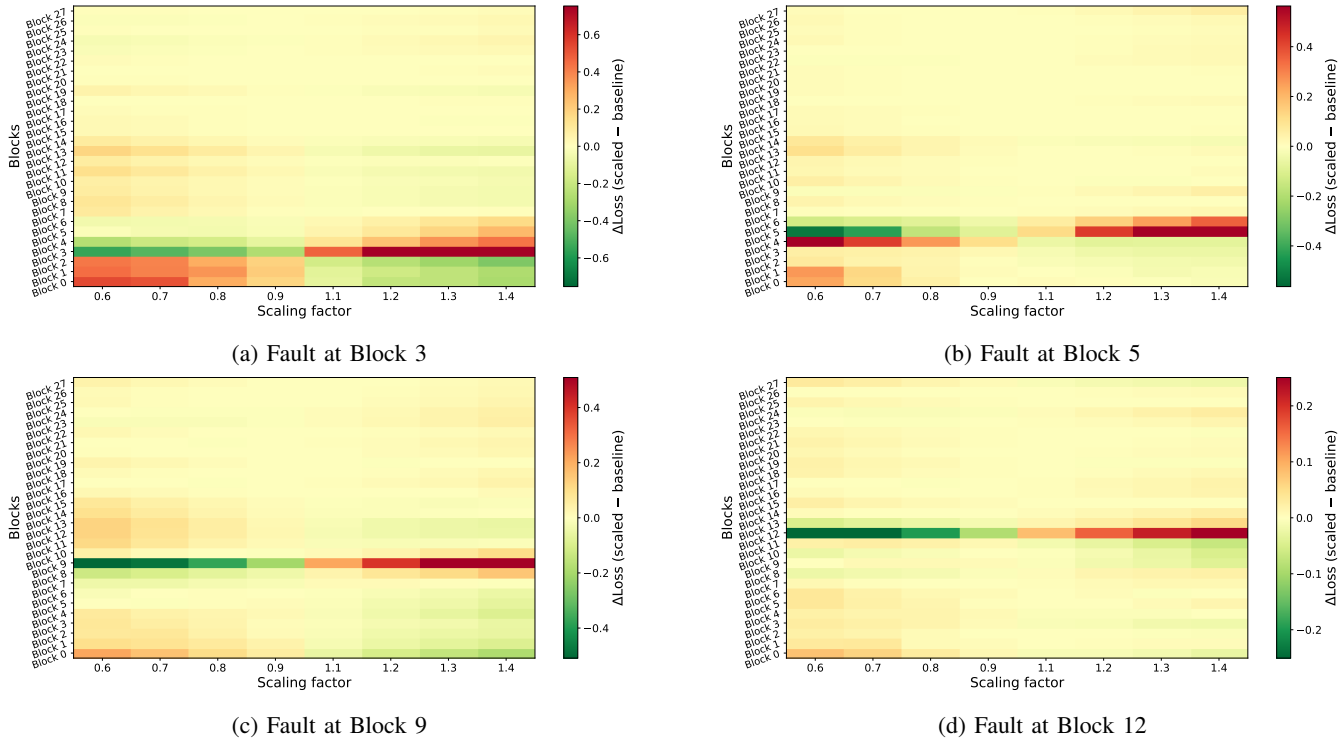


Fig. 5: Heatmaps of ΔLoss for LLaMA 3.2 3B across the four injected faults. The corrupted block in each case shows a pronounced asymmetric loss pattern under scaling.

followed by an analysis of recovery behavior and overall efficiency.

A. Self-Referential Fault Localization Results

We first evaluate the self-referential localization method on the LLaMA 3.2 3B model by injecting bit-flips into four critical blocks identified by GenBFA [6] (blocks 3, 5, 9, and 12). Fig. 5 shows the resulting heatmaps of ΔLoss across all blocks for the chosen scaling values. In each case, the corrupted block exhibits a distinctive asymmetric pattern: the loss sharply increases for $\alpha > 1$ and decreases for $\alpha < 1$, whereas non-faulty blocks show minimal or monotonic behavior. This strong contrast provides a clear signal for isolating the faulty block.

To quantify this behavior, we compute the Block Sensitivity Score (BSS) for each block. As shown in Fig. 6, the corrupted block consistently achieves the highest BSS across all four injected faults, while non-faulty blocks remain comparatively low. This demonstrates that the BSS metric reliably highlights the corrupted block under residual scaling.

To assess scalability, we repeat the same procedure on the larger LLaMA 3.1 8B model, injecting bit-flips into blocks 3, 9, 15, and 28. BitFlipScope again identifies the correct corrupted block in every case, exhibiting the same asymmetric ΔLoss pattern and dominant BSS score observed in the 3B model. Heatmaps and sensitivity plots for the 8B model are provided in Appendix A. These results demonstrate that

residual-path sensitivity generalizes consistently to deeper and larger LLM architectures.

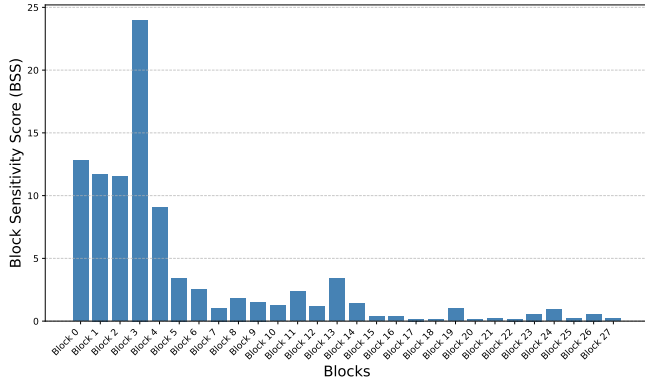
B. Differential Fault Localization Results

We evaluate BitFlipScope’s differential localization performance by injecting single bit-flips into both MLP and self-attention sublayers across multiple transformer blocks and model sizes. In this setting, the clean model serves as a behavioral reference, and localization is determined by identifying block and sublayer divergences between the clean and corrupted models. Table I summarizes the outcomes for the tested bit-flip locations.

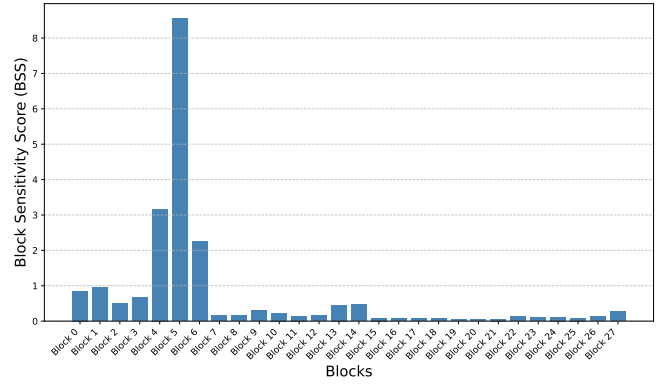
Model	Block	MLP (up/down)	Attention (Q/K/V)	Localized
1B	3	up, down	q, k, v	✓
1B	5	up, down	q, k, v	✓
1B	9	up, down	q, k, v	✓
3B	3	up, down	q, k, v	✓
3B	5	up, down	q, k, v	✓
3B	9	up, down	q, k, v	✓

TABLE I: Localization success for bit-flips injected into MLP (up/down) and Attention (Q/K/V) sublayers across model blocks.

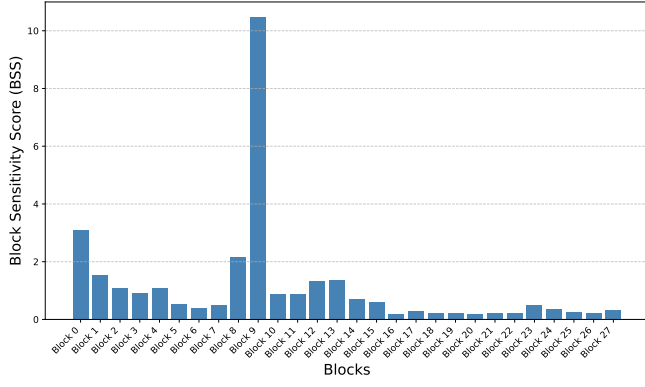
a) MLP Sublayers: Across all tested blocks and model sizes, BitFlipScope reliably localized faults injected into the up- and down-projection sublayers of the MLP module. These results show that activation discrepancies within the MLP stack are sufficiently distinctive to reveal corrupted parameters.



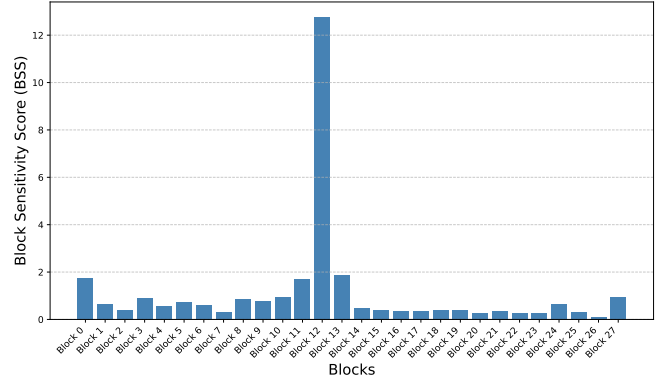
(a) Fault at Block 3



(b) Fault at Block 5



(c) Fault at Block 9



(d) Fault at Block 12

Fig. 6: Block Sensitivity Scores (BSS) for LLaMA 3.2 3B. In all cases, the corrupted block exhibits the highest sensitivity.

b) Attention Sublayers: Similarly, bit-flips introduced into the query, key, and value projections were consistently isolated. This is notable because Q/K/V projections are tightly coupled through the multi-head attention mechanism; nevertheless, the differential hidden-state comparison provides a clear fingerprint for identifying the corrupted subcomponent.

c) Generalization Across Models and Blocks: The consistent localization performance across different blocks (3, 5, and 9) and across two model sizes (1B and 3B) indicates that the differential method generalizes well with respect to architectural depth, scale, and parameter type.

1) Comparative Analysis with Brute Force: To contextualize BitFlipScope’s efficiency, we compare it against an exhaustive parameter differencing approach. A transformer with 16 blocks, each containing 7 tensors of size 16,777,216, requires:

$$16 \times 7 \times 16,777,216 = 1,879,419,392$$

elementwise comparisons.

By contrast, BitFlipScope performs:

- 16 hidden-state comparisons (block filtering),
- 2 activation comparisons (layer filtering),
- 3 hash computations (constant cost),
- 1 tensor-level comparison at the identified sublayer.

The total workload is therefore:

$$16 + 2 + 3 + 16,777,216 = 16,777,237,$$

a reduction of more than two orders of magnitude relative to brute-force search, demonstrating the computational scalability of our differential pipeline.

Method	Number of Computations
Brute Force	1,879,419,392
BitFlipScope	~16,777,237

TABLE II: Computation cost comparison between brute-force parameter differencing and BitFlipScope’s differential fault localization.

C. Performance Recovery Results

After localizing the corrupted block, we evaluate whether BitFlipScope enables practical, fine-tuning-free recovery in the self-referential setting. We mitigate the bit-flip fault by zeroing out the residual contribution of the identified faulty block, thereby suppressing its corrupted computation. Table III summarizes the resulting MMLU accuracy.

For the LLaMA 3.2 3B model, accuracy drops from 61% to 3.2% after a bit-flip but recovers to 51% after mitigation, restoring 82.7% of the lost performance. Similarly, for the LLaMA 3.1 8B model, accuracy recovers from 3.9% back

to 56%, recovering 80.0% of the degradation. These results demonstrate that once BitFlipScope identifies the corrupted block, inexpensive inference-time mitigation can substantially restore model behavior without retraining or a clean reference model.

In the differential setting, where a clean reference model is available, BitFlipScope enables full restoration of model functionality: replacing the corrupted weight tensor with its clean counterpart fully recovers baseline accuracy in every evaluated case.

Model	Baseline Accuracy	After Bitflip	After Recovery	Recovery Percentage
LLaMA 3B	61.0%	3.2%	51.0%	82.7%
LLaMA 8B	69.0%	3.9%	56.0%	80.0%

TABLE III: MMLU accuracy before attack, after bit-flip, and after recovery.

VI. CONCLUSION

This paper introduced **BitFlipScope**, a unified and scalable framework for localizing and mitigating bit-flip faults in large language models under two practical deployment settings: with and without access to a clean reference model. By leveraging differential behavioral analysis in the former case and residual-path sensitivity in the latter, BitFlipScope provides reliable and interpretable diagnostic signals that accurately localize corrupted blocks and sublayers while requiring orders of magnitude fewer computations than brute-force search. Our findings further show that identified faults can be effectively mitigated: targeted parameter replacement fully restores accuracy when a clean model is available, and inference-time attenuation recovers over 80% of lost performance in the self-referential setting without fine-tuning. These results demonstrate that scalable, software-only fault localization is both feasible and impactful for modern multi-billion-parameter models, laying the groundwork for more robust, secure, and self-diagnosing LLM deployments in safety-critical environments.

REFERENCES

- [1] M. Raza, Z. Jahangir, M. B. Riaz, M. J. Saeed, and M. A. Sattar, “Industrial applications of large language models,” *Scientific Reports*, vol. 15, Apr. 2025.
- [2] B. C. Das, M. H. Amini, and Y. Wu, “Security and privacy challenges of large language models: A survey,” *ACM Comput. Surv.*, vol. 57, Feb. 2025.
- [3] A. Almalky, S. Ahmed, R. Zhou, M. A. Nahian, A. A. Arafat, S. Angizi, and A. S. Rakin, “Llwra: Large language models weight replacement attack,” in *2025 International Conference on Control, Automation and Diagnosis (ICCAD)*, pp. 1–6, 2025.
- [4] F. Yao, A. S. Rakin, and D. Fan, “DeepHammer: Depleting the intelligence of deep neural networks through targeted chain of bit flips,” in *29th USENIX Security Symposium (USENIX Security 20)*, pp. 1463–1480, USENIX Association, Aug. 2020.
- [5] A. S. Rakin, Z. He, and D. Fan, “Bit-flip attack: Crushing neural network with progressive bit search,” in *2019 IEEE/CVF International Conference on Computer Vision (ICCV)*, pp. 1211–1220, 2019.
- [6] S. Das, S. Bhattacharya, S. Kundu, S. Kundu, A. Menon, A. Raha, and K. Basu, “Genbfa: An evolutionary optimization approach to bit-flip attacks on llms,” 2025.

- [7] Q. Liu, W. Wen, and Y. Wang, “Concurrent weight encoding-based detection for bit-flip attack on neural network accelerators,” in *Proceedings of the 39th International Conference on Computer-Aided Design, ICCAD ’20*, (New York, NY, USA), Association for Computing Machinery, 2020.
- [8] N. Nazari, H. M. Makrani, C. Fang, H. Sayadi, S. Rafatirad, K. N. Khasawneh, and H. Homayoun, “Forget and rewire: Enhancing the resilience of transformer-based models against Bit-Flip attacks,” in *33rd USENIX Security Symposium (USENIX Security 24)*, (Philadelphia, PA), pp. 1349–1366, USENIX Association, Aug. 2024.
- [9] Q. Liu, J. Yin, W. Wen, C. Yang, and S. Sha, “NeuroPots: Realtime proactive defense against Bit-Flip attacks in neural networks,” in *32nd USENIX Security Symposium (USENIX Security 23)*, (Anaheim, CA), pp. 6347–6364, USENIX Association, Aug. 2023.
- [10] F. Baradaran, M. Raji, A. Baradaran, A. Baradaran, and R. Akbarifard, “Zero memory overhead approach for protecting vision transformer parameters against bit-flip faults,” in *2025 29th International Computer Conference, Computer Society of Iran (CSICC)*, pp. 1–5, 2025.
- [11] M. AI, “Introducing Meta Llama 3: The most capable openly available llm to date.” <https://ai.meta.com/research/publications/introducing-meta-llama-3>, 2024. Accessed: 2025-02-15.
- [12] T. Feraco and E. Toffalini, “Sembeddings: how to evaluate model misfit before data collection using large-language models,” *Frontiers in Psychology*, vol. Volume 15 - 2024, 2025.
- [13] R. Zhuang, T. Wu, Z. Wen, A. Li, J. Jiao, and K. Ramchandran, “Embedllm: Learning compact representations of large language models,” Oct. 2024.
- [14] C. Qian, M. Zhang, Y. Nie, S. Lu, and H. Cao, “A survey of bit-flip attacks on deep neural network and corresponding defense methods,” *Electronics*, vol. 12, no. 4, 2023.
- [15] A. Vaswani, N. Shazeer, N. Parmar, J. Uszkoreit, L. Jones, A. N. Gomez, Ł. Kaiser, and I. Polosukhin, “Attention is all you need,” in *Advances in Neural Information Processing Systems (NeurIPS)*, 2017.
- [16] D. Hendrycks, C. Basart, S. Kadavath, M. Mazeika, A. Arora, E. He, N. Carlini, J. Schulman, D. Song, and J. Steinhardt, “Measuring massive multitask language understanding,” in *International Conference on Learning Representations (ICLR)*, 2021.
- [17] Y. Fan, Y. Hong, Q. Wang, J. Bao, H. Jiang, and Y. Song, “Preference-oriented supervised fine-tuning: Favoring target model over aligned large language models,” *Proceedings of the AAAI Conference on Artificial Intelligence*, vol. 39, pp. 23859–23867, Apr. 2025.

APPENDIX

A. Additional Self-Referential Results for LLaMA 3.1 8B

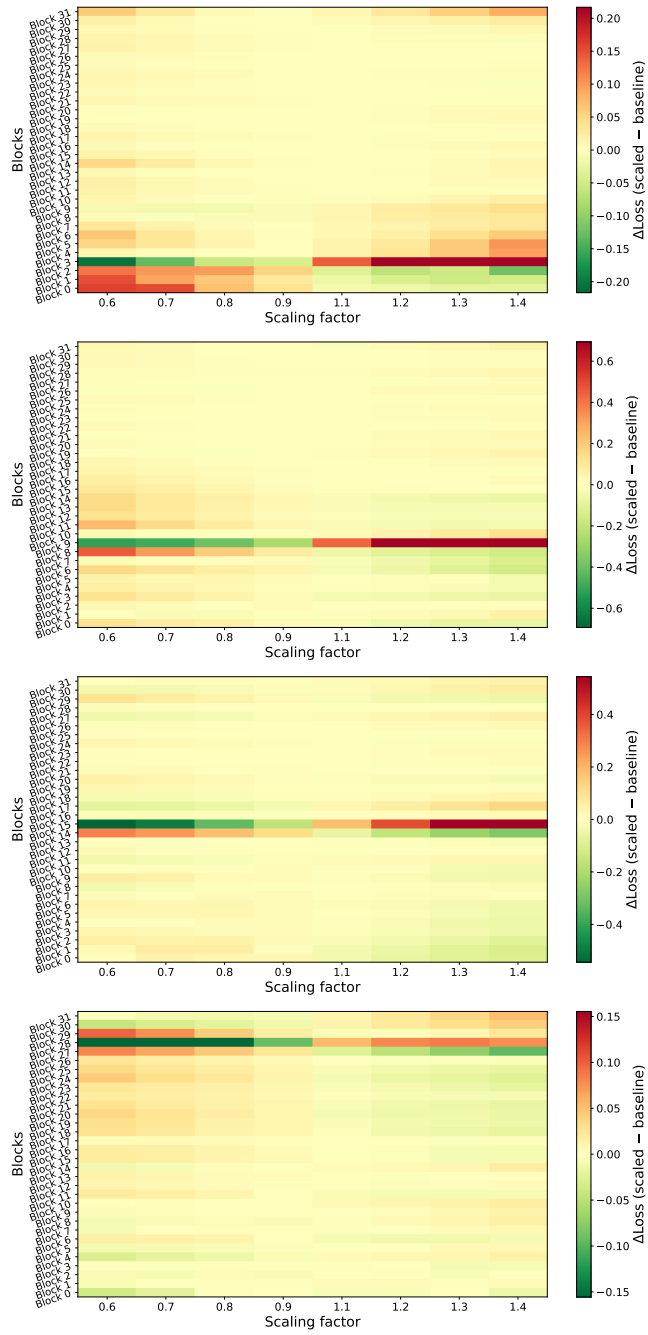


Fig. 7: Heatmaps of ΔLoss for LLaMA 3.1 8B across injected faults.

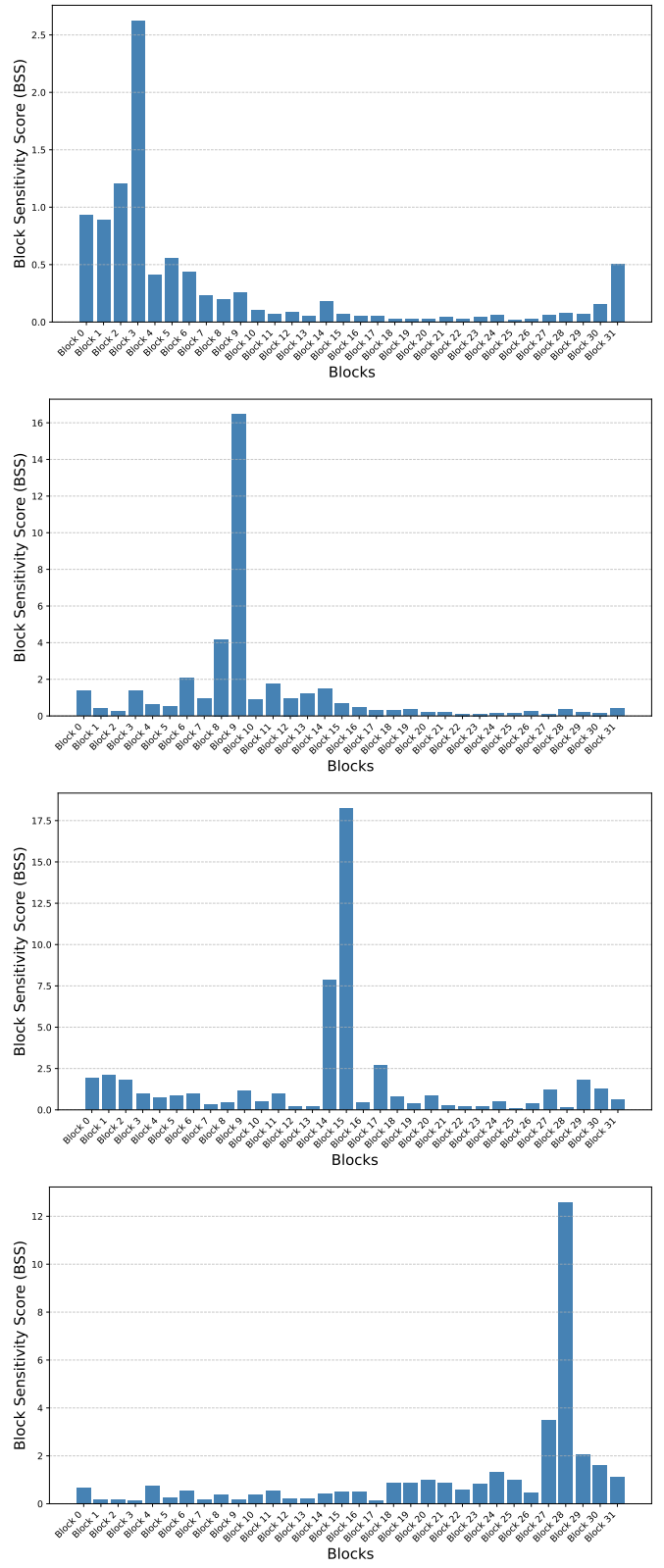


Fig. 8: Block Sensitivity Scores (BSS) for LLaMA 3.1 8B.